Drug Annotation

Discovery and Characterization of Clinical Candidate LXE408 as a Kinetoplastid-Selective Proteasome Inhibitor for the Treatment of Leishmaniases

Advait Nagle,* Agnes Biggart, Celine Be, Honnappa Srinivas, Andreas Hein, Diana Caridha, Richard J. Sciotti, Brandon Pybus, Mara Kreishman-Deitrick, Badry Bursulaya, Yin H. Lai, Mu-Yun Gao, Fang Liang, Casey J. N. Mathison, Xiaodong Liu, Vince Yeh, Jeffrey Smith, Isabelle Lerario, Yongping Xie, Donatella Chianelli, Michael Gibney, Ashley Berman, Yen-Liang Chen, Jan Jiricek, Lauren C. Davis, Xianzhong Liu, Jaime Ballard, Shilpi Khare, Fabian Kurt Eggimann, Alexandre Luneau, Todd Groessl, Michael Shapiro, Wendy Richmond, Kevin Johnson, Patrick J. Rudewicz, Srinivasa P. S. Rao, Christopher Thompson, Tove Tuntland, Glen Spraggon, Richard J. Glynne, Frantisek Supek, Christian Wiesmann,* and Valentina Molteni*

Cite This: *J. Med. Chem.* 2020, 63, 10773−10781

Read Online

ACCESS | Metrics & More | Article Recommendations | Supporting Information

ABSTRACT: Visceral leishmaniasis is responsible for up to 30,000 deaths every year. Current treatments have shortcomings that include toxicity and variable efficacy across endemic regions. Previously, we reported the discovery of GNF6702, a selective inhibitor of the kinetoplastid proteasome, which cleared parasites in murine models of leishmaniasis, Chagas disease, and human African trypanosomiasis. Here, we describe the discovery and characterization of LXE408, a structurally related kinetoplastid-selective proteasome inhibitor currently in Phase 1 human clinical trials. Furthermore, we present high-resolution cryo-EM structures of the *Leishmania tarentolae* proteasome in complex with LXE408, which provides a compelling explanation for the noncompetitive mode of binding of this novel class of inhibitors of the kinetoplastid proteasome.

Inhibitors bound to β5 subunit of *L.tarentolae* proteasome

1, LXE408

Bortezomib

LXE408
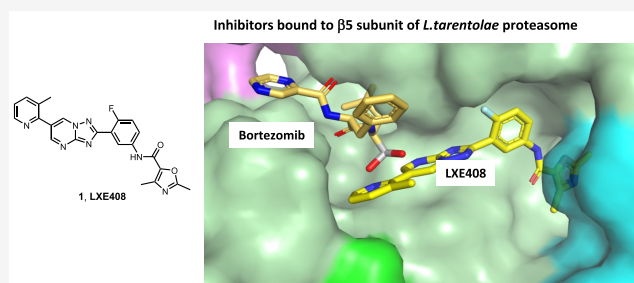
INTRODUCTION

Visceral leishmaniasis (VL) is an infectious disease causing 50,000−90,000 new cases and 30,000 deaths every year.[1] In the Indian subcontinent, the first-line treatment for this infection is a single infusion of AmBisome (liposomal amphotericin B). However, liposomal amphotericin B has limited efficacy in East Africa both as a monotherapy and in combination with other drugs;[2] therefore, in this endemic area the first line of treatment is a 17-day therapy with antimony stibogluconate and paromomycin combination.[3,4] Overall, existing parenteral treatments are difficult to administer, require hospitalization, and have dose-limiting toxicities.[5] New drugs that are orally bioavailable, safe and can effect rapid cure are necessary to address needs of VL patients in developing economies.

Previously, we reported the identification of a novel pan-kinetoplastid growth inhibitor series, exemplified by GNF6702, and demonstrated that this triazolopyrimidine scaffold exerts its antiparasitic activity through selective inhibition of kinetoplastid proteasome chymotrypsin activity.[6] Subse-

quently, a GSK/University of Dundee group reported the discovery of a structurally related scaffold, as well as its unique binding mode to *Leishmania tarentolae* proteasome, explaining the scaffold's exceptional selectivity for the kinetoplastid compared to the mammalian proteasome.[7] Here, we describe the optimization of GNF6702 that led to the selection of **1** (LXE408), a compound with remarkable efficacy in murine models of visceral and cutaneous leishmaniasis that is currently in Phase 1 human clinical trials. We also disclose the high-resolution cryo-EM costructure of **1** with the *Leishmania tarentolae* proteasome in the presence of the prototypical competitive proteasome inhibitor bortezomib which clarifies

Table 1. In Vitro Data for Key Analogues
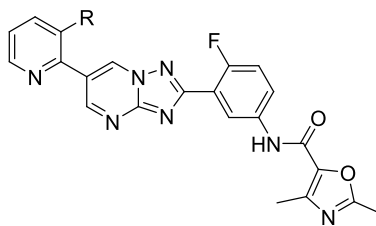
compound no.	R group	L. donovani proteasome IC$_{50}$ (μM)[a]	L. donovani EC$_{50}$ (μM)[b]	HT sol. pH 6.8 (μM)[c]	ER[d] mouse/rat/dog/human	mp temp (°C)
1 (LXE408)	Me	0.04	0.04	17	<0.21/<0.18/<0.24/0.27	139
2 (GNF6702)	H	0.035	0.02	10	<0.21/<0.27/0.46/0.3	224
3	CHF$_2$	0.06	0.11	21	0.51/<0.18/0.57/0.55	n.t.
4	Cl	0.1	0.05	7	<0.21/n.t. /<0.21/0.21	229
5	OMe	n.t.	0.07	7	0.4/n.t./0.56/<0.21	n.t.
6	CH$_2$OH	0.07	0.5	n.t.[e]	n.t./n.t./n.t./n.t.	n.t.

[a]Half-maximum inhibition of chymotrypsin-like activity of purified *L. donovani* proteasome. [b]Half-maximum inhibition of *L. donovani* amastigote proliferation within primary mouse macrophages. [c]Solubility determined in a high-throughput assay format. [d]Microsomal extraction ratio. The assay measures the amount of parent compound remaining after 1 h incubation in microsomes. [e]n.t. = not tested. IC$_{50}$ and EC$_{50}$ values correspond to means ($n = 4$ technical replicates).

the noncompetitive nature of proteasome inhibition for this novel class of antileishmanial agents.[6]

RESULTS AND DISCUSSION

The progression of GNF6702 (**2**) into clinical testing was hampered by solubility-limited oral absorption. While this limitation could have potentially been addressed by a specialized formulation (e.g., nanosuspension, solid dispersion), such an approach would likely increase the cost of treatment and complicate its use in developing economies. As a result, we set out to perform medicinal chemistry optimization of GNF6702 in order to identify a development candidate with improved solubility and improved oral exposure across preclinical species. Initial efforts, focusing on reducing logP and increasing the sp^3 fraction to increase solubility, led to molecules with less potency or high clearance. A solubility analysis pointed to the high crystal packing energy of GNF6702 (melting point = 224 °C) as the key solubility-limiting issue.[8] As the molecule was quite planar, we decided to introduce small substitutions at the pyridine 3-position (R) to force the pyridine out of plane with respect to the bicyclic core in an effort to reduce the crystal packing energy and thus improve solubility (Table 1).[9]

In general, the compounds synthesized with different R groups maintained an inhibitory activity on purified *L. donovani* proteasome similar to the unsubstituted compound **2**. Compounds **1** and **4** emerged as frontrunners, having good potency in the more relevant intracellular *L. donovani* growth inhibition assay and favorable microsomal stability across species. Finally, using the melting point temperature as an indicator of crystal packing energy, we selected compound **1** over compound **4** for further characterization due to its lower melting point temperature (melting point = 139 °C). A salt and form selection screen was conducted on compound **1** (22 different counterions and cocrystal formers in 4 solvents). The fumarate (cocrystal) was selected as the preferred candidate exhibiting appropriate properties in terms of stability, solubility, and excipient compatibility. The melting point of the thermodynamically stable polymorph fumarate cocrystal was 224 °C.

In a dissolution study, the fumarate cocrystal of **1** showed a significantly higher dissolution rate than the free base of **2** (see Figure 1). Furthermore, previous studies have shown that
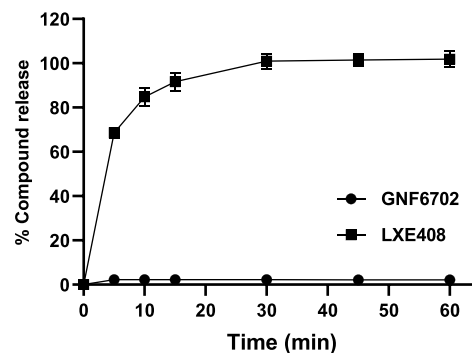

Figure 1. Time course of dissolution of **1** (LXE408, fumarate cocrystal) vs **2** (GNF6702).

compounds with higher supersaturation stability in fasted state simulated intestinal fluid (FASSIF) display better absorption in the intestine.[10] When compared to free base of compound **2**, fumarate cocrystal of compound **1** was found to maintain a 5-fold higher supersaturation in FASSIF achieving a concentration of 73 μM at 16 min.[11] It should be noted that no suitable salt or cocrystal form of compound **2** with the right properties could be identified upon screening with various counterions. Overall, the data presented supported our decision to select compound **1** (LXE408) for further characterization.

To determine efficacy in vivo, compound **1** was administered for 8 days at three dose levels in a murine model of VL. In mice infected with *L. donovani*,[12] oral dosing (PO) with **1** effected a more pronounced reduction in liver parasite burden than miltefosine, the only oral antileishmanial drug available in clinical practice (Figure 2a). Dosing compound **1** at 1 mg/kg b.i.d. led to a 95% reduction of parasite burden in the liver, an efficacy equivalent to that effected by a 12 mg/kg q.d. regimen of miltefosine. This miltefosine regimen yielded plasma exposures in mice similar to the miltefosine clinical regimen.
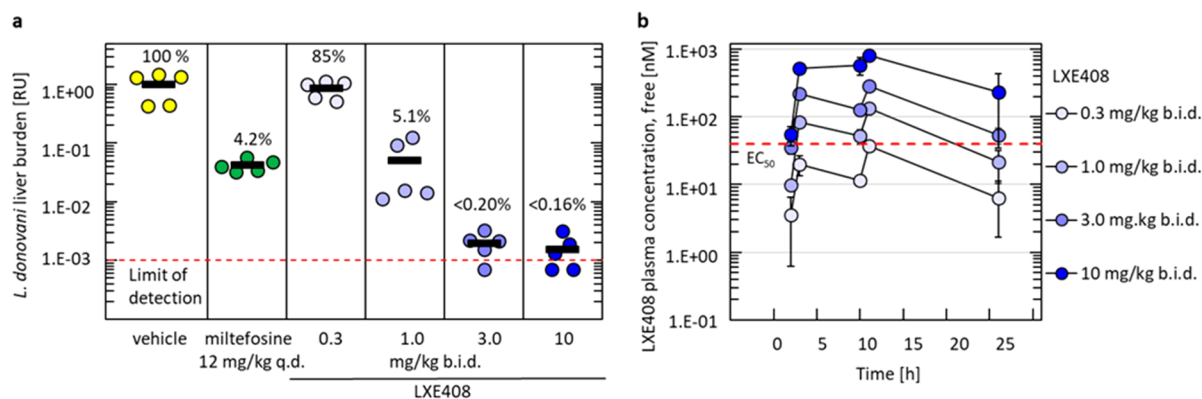
Figure 2. a) Compound **1** post-treatment *L. donovani* liver burdens in a murine model of VL as assessed by qPCR. Circles: burdens in individual mice; thick horizontal lines: means of the treatment groups; red dotted line: limit of *L. donovani* detection by qPCR; circles below the red dotted line: mice with no detectable *L. donovani* parasites; RU: relative units. Data points below the limit of detection are "jittered" to show the number of animals in the group. b) Time profiles of mean free plasma concentration of compound **1**; free compound **1** concentration values were predicted from measured total plasma concentration values collected on day 8 of treatment. Dashed red line corresponds to intramacrophage *L. donovani* EC$_{50}$ of 40 ± 8.1 nM. Circles: means ± SD; $n = 5$ mice; fraction unbound in mouse plasma = 0.056. For data points lacking error bars, standard deviations are smaller than circles the representing means.

The in vivo efficacy of compound **1** plateaued at the 3 mg/kg b.i.d. dose with no further reduction of liver parasite burden at the 10 mg/kg b.i.d. dose. The plasma exposure of **1** increased dose-proportionally, and the free plasma concentration of **1** (mouse plasma protein binding = 94.4%) at the 3 and 10 mg/kg b.i.d. doses was above the EC$_{50}$ value of **1** on intramacrophage *L. donovani* amastigotes throughout the duration of treatment (Figure 2b). This observation is consistent with our previously published PK-PD model for this class of compounds, which indicated that the proteasome inhibitor efficacy is driven by free AUC and/or by time above C$_{min.}$[6] Such a PK-PD profile suggests that sustained inhibition of the parasite proteasome, which results in intracellular accumulation of ubiquitylated proteins, is required for rapid clearance of *L. donovani* in vivo.

Next, we tested the in vivo efficacy of **1** in a murine model of cutaneous leishmaniasis (CL). In BALB/c mice infected with *L. major* (a model of Old World leishmaniasis), oral dosing with **1** effected robust healing of parasite-induced skin lesions at the base of the tail. Administration of **1** for 10 days at a dose of 20 mg/kg b.i.d. produced a therapeutic effect comparable to that of liposomal amphotericin B, the most potent anti-leishmanial drug available today for CL therapy (Figure 3). Previously, we showed that compound **2** had superior antiparasitic activity in BALB/c footpad model of *L. major* infection when compared to miltefosine.[6] Data presented here further extend these findings and establish **1** as a promising oral agent for treatment of cutaneous leishmaniasis.

Compound **1** was profiled in vitro for off-target activity on a panel of receptors including GPCRs, nuclear receptors, and kinases. For VMAT2, 61% inhibition was observed at 10 μM concentration; however, compound **1** had a low propensity to cross the blood brain barrier (brain/plasma AUC ratio = 0.03 in mice) suggesting minimal potential modulation of the VMAT2 receptor in the brain. Overall, compound **1** was not considered to pose a risk of off-target activity at clinically relevant concentrations (see the Supporting Information). In addition, the compound also showed no inhibition of the hERG channel (IC$_{50}$ > 30 μM) in a manual patch clamp assay indicating a low risk for QT prolongation. Finally, in vitro
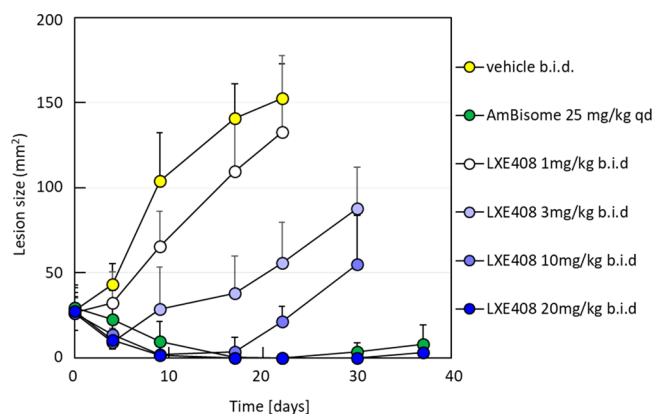

Figure 3. Efficacy of **1** in the BALB/c mouse model of Old World leishmaniasis. Data in the graph show progression of lesion sizes at the base of the tail of BALB/c mice infected with 1×10^7 *L. major* parasites after 10 days of treatment. Experimental time points represent the mean lesion sizes ± SEM ($n = 6$). Single-factor ANOVA (Dunnet's test) was used to determine the statistical significance of differences in lesion sizes between vehicle and compound-treated groups ($P < 0.05$). Starting from day 4 post-treatment, lesion sizes in the vehicle control group were bigger and statistically differed from lesion sizes in compound-treated groups except for the compound **1** at 1 mg/kg b.i.d. dose.

AMES and in vivo micronucleus (MNT) studies in rat did not indicate a risk of mutagenicity or clastogenicity, respectively.

Pharmacokinetic studies in selected preclinical species (mouse, dog, rat, and cynomolgus monkey) using the fumarate salt (Table 2) revealed that **1** had low clearance (CL, 2−17% of hepatic blood flow) and low steady-state volume of distribution values (V$_{ss}$, smaller or comparable to the volume of total body water) in mouse, rat, and monkey following intravenous (IV) compound administration. However, the CL and V$_{ss}$ values in dog were in the moderate range (CL: 37% of hepatic blood flow and V$_{ss}$ larger than the total volume of body water). The plasma terminal half-life of **1** was in the range of 3−10 h across species following IV administration. Oral bioavailability was 27−67% across the tested species when using conventional suspension formulations.

Table 2. Pharmacokinetic Profile of Compound 1 in Selected Preclinical Species

PK parameters	mouse[a]	rat[b]	dog[c]	monkey[d]
CL (mL/min/kg)	2.3	2.1	11.6	0.9
V_{ss} (L/kg)	0.63	0.53	2.1	0.5
$T_{1/2}$ IV (h)	3.3	3.8	3.8	9.7
MRT IV (h)	4.6	4.3	3.3	9.7
DN AUC PO (h·μM)	7.5	12	1.5	12
DN C_{max} PO (μM)	0.8	1.0	0.3	1.0
F (%)	46	67	44	27

[a]Balb/C mice, 5 mg/kg IV and 20 mg/kg PO doses. [b]Male Sprague–Dawley rat, 3 mg/kg IV and 10 mg/kg PO doses. [c]Male beagle dog, 0.3 mg/kg IV and 1.0 mg/kg PO doses. [d]Male cynomolgus monkey, 0.3 mg/kg IV and 10 mg/kg PO doses. For IV dosing, 1 was formulated in 75% PEG300/25% D5W vehicle; for PO dosing, 1 was formulated in 0.5% methylcellulose, 0.2% Tween 20 vehicle; CL: plasma clearance after administration of a single IV bolus dose; V_{ss}: volume of distribution at steady-state; DN AUC PO: dose-normalized area under the plasma concentration−time curve after administration of a single oral dose; DN C_{max} PO: dose-normalized maximum plasma concentration after administration of a single oral dose; F (%): oral bioavailability after administration of a single oral dose.

In order to select the preclinical species for toxicology studies that would reflect most closely the metabolism of 1 in human, we identified and quantified the most abundant metabolites in in vitro hepatocytes and in vivo. In vitro, 1 was mainly metabolized to monohydroxylated metabolites 6−8 (see Figure 4). Metabolite 6 showed a modest activity of 0.5 μM on parasites, whereas the other two metabolites had an activity of greater than 5 μM. No unique metabolites were detected in human hepatocytes. While the metabolism profile of 1 was qualitatively similar across the tested species, we observed species differences in the extent of formation of individual metabolites. The predominant metabolite in dog hepatocytes was 8 with minor formation of the other two metabolites (6 and 7). In contrast, in mouse, rat, monkey, and human hepatocytes, the predominant metabolite was 7 with minor formation of the other two metabolites (6 and 8).

The in vivo metabolic profiles of 1 in mouse, rat, dog, and monkey plasma after oral administration were consistent with the in vitro hepatocytes data (Table 3). After a single oral dose, the exposure of metabolite 8 was higher than that of 1 in dog plasma (120%), while it was minor (0.2−5%) in plasma of all the other species (see Table 4). Levels of 6 and 7 were in moderate or low range in dog plasma (≤10% of parent). In mouse, rat, and monkey plasma, 6 was less than 10% relative to the equivalent exposure of 1, and 7 was in the range of 5−17% of parent exposure. It is worth noting that the aniline resulting from amide hydrolysis was not detected in vivo. Using a panel of dog recombinant CYP enzymes, we performed P450 phenotyping studies that demonstrated that 1 was metabolized

Table 3. Distribution of Metabolites in Various Preclinical Species[a]

	abundance[a]				
	mouse	rat	dog	monkey	human
1	+++	+++	+++	+++	+++
6	+	+	+	+	+
7	+	+	+	+	+
8	n.d.	+	++	+	+

[a]Semiquantitative metabolite profiles were obtained after incubation of 10 μM of 1 for 4 h and analysis using UV chromatographic data (250 nm). All integrable peaks were normalized to the percent area of the largest observed peak. +++ > 75%; ++ ≤ 75%>25%; + ≤25%.

Table 4. Percentage of Metabolite Exposure Relative to 1 in Preclinical Species Following Oral Administration at 10 mg/kg
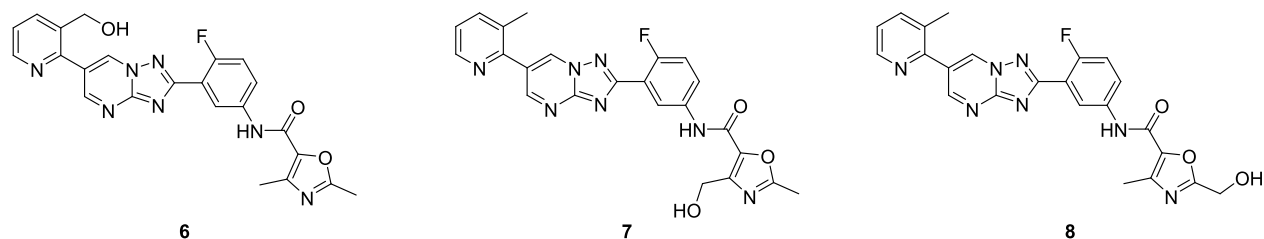
	metabolites (%)[a,b]		
species	6	7	8
mouse	1.5	4.5	0.2
rat	1.5	17	1.5
dog	9.1	2.3	120
monkey	1.7	11	5.1

[a]AUC of metabolites was dose-normalized before relative amounts were calculated. [b]The concentrations were analyzed from experiments described in Table 2.

to 8 predominantly by CYP2D15 in dog. Importantly, compound 1 was not a substrate of human CYP2D6, the human ortholog of dog CYP2D15. Human recombinant CYP phenotyping experiments showed that CYP3A4, CYP1A1, 1A2, and 2J2 were the major enzymes responsible for the formation of metabolite 8. These data suggested that the metabolism in dog was not predictive of human metabolism, and therefore, monkey was selected as the nonrodent species for toxicological studies.

To further characterize compound 1, we wanted to establish its mode of binding to the proteasome.

Previously published mechanism of action studies indicated that 2 is an inhibitor of the kinetoplastid proteasome that selectively inhibits the chymotrypsin-like activity of the β5 proteasome subunit (PSMB5). In a biochemical assay, 2 inhibited the chymotrypsin-like activity in a noncompetitive manner when the fluorogenic peptide Suc-LLVY-[Rh110]-[Dpro] was used as the substrate. This observation, together with the identified resistant mutations in the β4 proteasome subunit (PSMB4), pointed to a potential binding site for 2 at the interface of the PSMB4 and PSMB5 subunits.[6] However, the exact binding site of 2 and how the compound binding mode relates to its noncompetitive mode of inhibition remained unanswered.[7] To this end, we elucidated the atomic

Figure 4. Compound 1 main oxidative metabolites.

structure of **1** in complex with the 20S proteasome from *L. tarentolae* using cryo-EM (Figure 6a). The resultant 3.4 Å resolution structure revealed a clearly defined density for compound **1** (Figure 6b) with **1** situated within the active site pocket of PSMB5 partly formed by the side chains of Ile29 and Phe24 of the PSMB4 subunit (Figure 6c).[13] There, the dimethyl-oxazole unit of **1** packs tightly with the two hydrophobic residues. The conformation is analogous to the one recently published by Wyllie et al.[7] and is in agreement with binding profiles from parasite resistant mutations. First, the β5 Y113F mutation of *T. brucei* proteasome leads to loss of activity for compound **1** (Supporting Information; 113 refers to the amino acid position in the mature β5 subunit), and second, the F24L mutation of the *L. tarentolae* proteasome exhibits a significant upshift in the IC_{50} value in response to the inhibitor (Figure 5). This is in contrast to the binding curve for
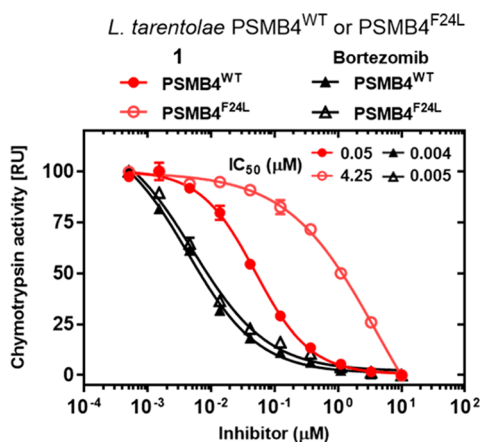

Figure 5. F24L mutation in proteasome β4 subunit confers selective resistance to **1**. Inhibition of chymotrypsin-like activity of purified wild-type ($PSMB4^{WT}$) and $PSMB4^{F24L}$ *L. tarentolae* proteasome by **1** and bortezomib; IC_{50} values of chymotrypsin-like activity are listed inside the plot. Data shown represents the means from one of the representative experiments ($n = 3$ technical replicates). RU (relative units) corresponds to the percentage of chymotrypsin-like activity relative to the DMSO control.

bortezomib (Figure 5) which shows no reduction in activity in response to the resistant mutation. Bortezomib is a prototypical peptidomimetic inhibitor of the proteasome, which inhibits proteasome chymotrypsin-like activity competitively with peptide substrates such as Suc-LLVY-[Rh110]-[Dpro]. This lack of resistance is in complete agreement with a large number of structural and biochemical studies of bortezomib in homologous proteasomes.[14]

However, when the structure of the canonical bortezomib binding mode is superimposed with the structure of the binary complex with **1**, steric clashes indicate that **1** and bortezomib cannot bind to the PSMB5 pocket simultaneously without a conformational change in the pocket for one or both of the compounds. To understand this at an atomic level, a cryo-EM structure of the ternary complex with *L. tarentolae* proteasome in the presence of **1** and bortezomib was solved. The resulting proteasome structure, solved at 3.2 Å resolution, clearly revealed that both **1** and bortezomib can occupy the pocket as a ternary complex with the proteasome. The binding mode of **1** remained unchanged when compared to the binary complex between the compound and the proteasome. In contrast, bortezomib adopted a novel conformation with its phenyl

group rotated ∼60 degrees around the dihedral angle connection formed by the phenyl with the bortezomib backbone when compared to the previously published crystal structures of the human proteasome in complex with bortezomib (Figure 7a and 7b).[13] Overall, these findings provide atomic level resolution details of the binding of **1** to the kinetoplastid proteasome and explain its noncompetitive mode of chymotrypsin-like activity inhibition.

Chemical Synthesis of Compound 1. Scheme 1 outlines the research synthesis of compound **1** that was achieved in 8 steps with an overall 8% yield. The synthesis was initiated from commercially available 2-fluoro-5-nitrobenzoic acid **9**, which upon treatment with thionyl chloride was converted to acid chloride. The excess thionyl chloride was removed under reduced pressure to be used for next step. The crude acid chloride was resuspended in toluene, and the intermediate was treated with aminoguanidine carbonate for 12 h, which yielded **10** as a solid. Amino guanidine intermediate **10** was stirred in water at 100 °C for 8 h to yield the amino-triazole **11** in 51% yield. Triazole **11** was condensed with bromomalonaldehyde, and the resulting nitro compound was further reduced with Raney nickel in the presence of zinc iodide to afford the key intermediate **12**. The resulting amide from coupling of aromatic amine **12** with 2,4-dimethyl oxazole carboxylic acid was further functionalized to boronic ester using a Miyaura Borylation reaction.[15] Finally, Suzuki coupling between the boronic acid and 2-bromomethylpyridine gave the desired compound **1**.

CONCLUSIONS

The current target product profile for a new antileishmanial drug is to be safe, effective, and oral with a short course of treatment (<11 days).[16] Optimization of GNF6702 successfully led to compound **1** (LXE408) which, when dosed orally, demonstrates excellent efficacy in mouse disease models and has an appropriate safety profile in preclinical species. Applying the PK-PD principles, we expect that a dose of 85−190 mg per day will effect cure in VL patients. Currently, phase I studies in healthy human volunteers are ongoing to determine safety and tolerability. The compound will most likely be dosed in combination with other agents once the safety and efficacy is established in humans as a single agent. Cryo-EM efforts led to a detailed understanding of the mechanism of inhibition of chymotrypsin activity by **1** and elucidated a novel mode of binding. The discovery of the noncompetitive specific β5 proteasome inhibition and further understanding of the binding mode of **1** could prove to be transformative in the fields of infectious diseases and oncology where more subunit-selective proteasome inhibitors are being sought.[17,18]

EXPERIMENTAL SECTION

Materials and Methods. Commercially available starting materials were used as supplied without further purification. Reactions were carried out by using dry organic solvents (DCM, ACN, DMF, etc.) unless otherwise noted. Reactions were monitored using thin layer chromatography and an Agilent Technologies 1200 series 6140 Quadrupole LC-MS with UV detection at 254 nm in electrospray ionization (ESI) mode. For LC-MS, all retention times reported are at 254 nm UV channel unless otherwise noted. All NMR spectra were recorded on a Bruker AVANCE-400 spectrometer operating at a frequency of 400.13 MHz for ^{1}H and 100.61 MHz for ^{13}C equipped with a 5 mm QNP cryoprobe with Z-gradient. Chemical shifts for ^{1}H and ^{13}C spectra were referenced to residual solvent. MS were obtained on an Agilent Technologies 1200 series 6140 quadrupole
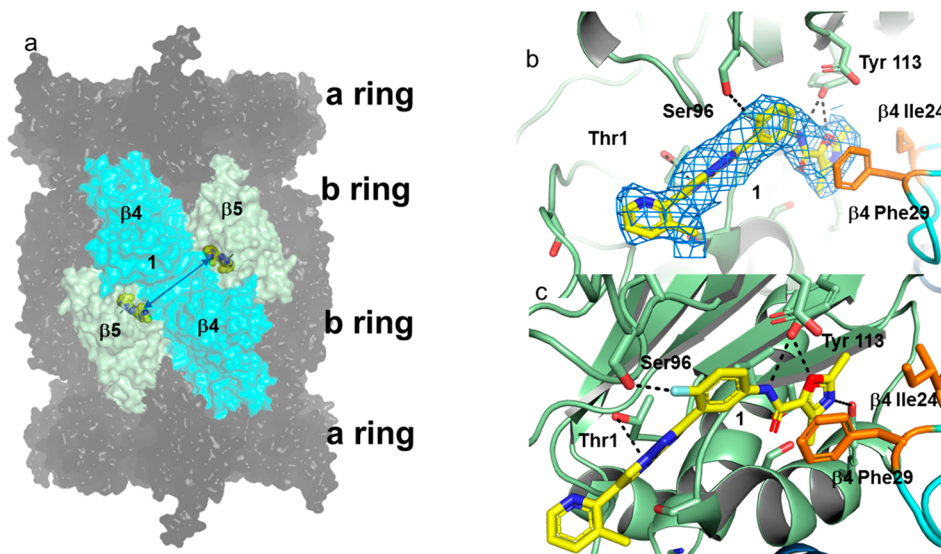
Figure 6. Binding of **1** to *L. tarentolae* proteasome. a) Positions of the two compound **1** molecules in the β5 subunit of proteasome, related β5 domains colored cyan, β4 subunits colored green. Compound **1** carbon atoms colored as yellow spheres. b) Electron density of the 3.4 Å structure around compound **1** (at 3 sigma deviations above the mean. EMDB and PDB code: EMD-10472, PDB ID 6TCZ. c) Key interactions around compound **1**, with resistance mutants in β4 subunit colored as orange sticks.
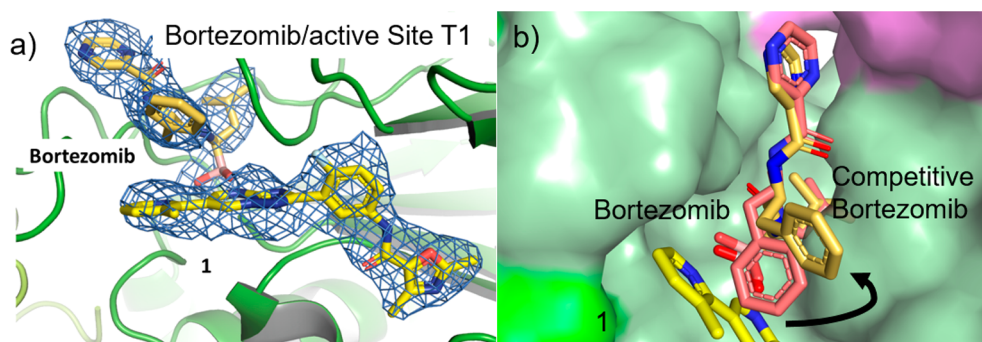

Figure 7. a) Final density map of the ternary complex of compound **1** and bortezomib bound to the β5 pocket. The map is displayed as a blue isomesh contoured at 3.0 σ above the mean, and for clarity it is displayed only around the ligands at a radius of 2.0 Å. The β5 chain is colored green in a cartoon representation; **1** and bortezomib are represented as sticks with carbons colored as yellow and beige, respectively. b) Rotation of bortezomib when competing with **1**, bortezomib in beige, **1** in yellow, relative to bortezomib. *Leishmania tarentolae* proteasome 20S subunit complexed with **1** and bortezomib accession code(s): EMD-10463, PDB ID: 6TD5.

Scheme 1. Synthesis of Compound 1[a]
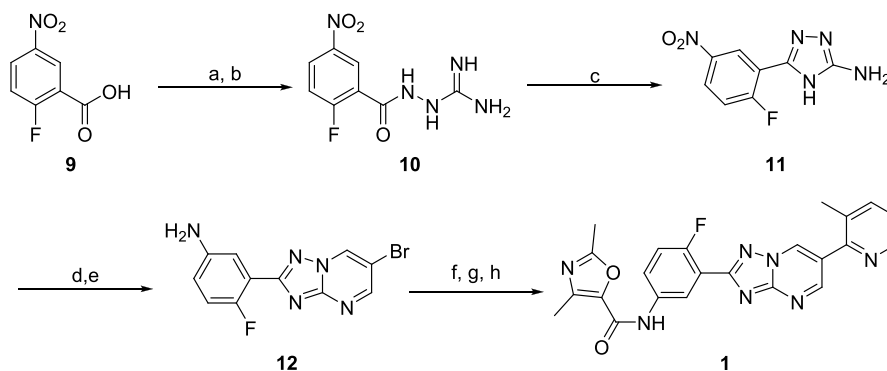
[a]Reagents and conditions. (a) SOCl₂, 80 °C, 4 h, 98%; (b) aminoguanidine carbonate, toluene, room temp 12 h, 97%; (c) H₂O, AcOH-carboxylic acid, HATU, DIEA, DMF, 0.5 h, 53%; (d) bromomalonaldehyde, AcOH, 100 °C, 43% (e) raney nickel, ZnI₂, THF, H₂ @ 50 psi, 2 h, 77% (f) 2,4-dimethyloxazole-5-carboxylic acid, HATU, DIEA, DMF, 0.5 h, 53%; (g) 4,4,4′,4′,5,5,5′,5′-octamethyl-2,2′-bi (1,3,2-dioxaborolane), Pd(dppf)Cl₂, KOAc, dioxane, 100 °C, 16 h, 24%; and (h) 2-bromo-3-methylpyridine, Pd(dppf)Cl₂, 1M, aq Na₂CO₃, 80 °C, 16 h, 39%.

LC-MS in electrospray ionization (ESI) mode. HRMS-ESI data were recorded using an Agilent 6520 Accurate-Mass Q-TOF LC-MS system with HPLC-Chip Cube interface and an Agilent 1200 HPLC. All final compounds were isolated analytically pure, >99% purity by

HPLC unless otherwise indicated. More information can be found in the Supporting Information.

2-(2-Fluoro-5-nitrobenzoyl)hydrazine-1-carboximidamide (10). A solution of 2-fluoro-5-nitrobenzoic acid (50 g, 270 mmol) in thionyl chloride (100 mL) was heated to 80 °C and stirred for 4 h. The mixture was allowed to cool down to room temperature, and the solvent was removed to give acid chloride intermediate (54 g, 98% yield).

To a solution of aminoguanidine carbonate (36.2 g, 266 mmol) in dry toluene (300 mL) cooled to 0 °C was added the above acid chloride (54 g, 266 mmol) over 30 min. The mixture was stirred at room temperature for 12 h. The formed precipitate was removed by filtration, and the residue was treated with H_2O (400 mL) and made alkaline with sodium carbonate. The solid was collected and recrystallized from water to obtain compound **10** (62 g, 97% yield). LCMS: [ESI] m/z = 241.1 [M + H]$^+$. The synthesis of the compound has been described previously and is commerically available.

5-(2-Fluoro-5-nitrophenyl)-4H-1,2,4-triazol-3-amine (11). A solution of compound **10** (62 g, 257 mmol) in H_2O (800 mL) was stirred for 8 h at 100 °C. After cooling, the solid obtained was filtered, and the cake was washed with H_2O (100 mL) and THF (100 mL) and dried to give **11** (34 g, 51% yield). ^{1}H NMR (400 MHz, DMSO) 12.42 (s, 1H), 8.74 (dd, J = 6.27 Hz, 3.0 Hz, 1H), 8.26 (dt, J = 7.0 Hz, 3.4 Hz, 1H), 7.57 (t, J = 9.5 Hz, 1H), 6.29 (s, 2H). ^{13}C NMR (101 MHz, DMSO) δ 164.34, 161.71, 157.72, 144.42, 144.39, 125.76, 125.66, 125.25, 125.20, 118.85, 118.61. HRMS found [M + H]$^+$ = 224.0578, $C_8H_7O_2N_5F$ predicted [M + H]$^+$ = 224.0578.

3-(6-Bromo-[1,2,4]triazolo[1,5-a]pyrimidin-2-yl)-4-fluoroaniline (12). To a solution of compound **11** (10 g, 44.8 mmol) in acetic acid (50 mL) was added 2-bromomalonaldehyde (8.12 g, 53.8 mmol) at room temperature. The mixture was heated to 100 °C and stirred for 4 h. The mixture was allowed to cool to room temperature before adding water (100 mL) and filtering. The filter cake was then washed with THF and dried under vacuum to give compound 6-bromo-2-(2-fluoro-5-nitrophenyl)-[1,2,4]triazolo[1,5-a]pyrimidine (6.5 g, 43% yield). ^{1}H NMR (400 MHz, DMSO) 10.04 (s, 1H), 9.08 (s, 1H), 8.96–9.04 (m, 1H), 8.47 (dt, J = 9.0 Hz, 3.4 Hz, 1H), 7.76 (t, J = 9.5 Hz, 1H). ^{13}C NMR (101 MHz, DMSO) δ 165.01, 162.36, 160.38, 157.47, 154.11, 144.68, 138.27, 138.09, 128.47, 128.36, 126.51, 126.46, 119.54, 119.36, 119.30, 107.08. HRMS found [M + H]$^+$ = 337.9688, $C_{11}H_6O_2N_5BrF$ predicted [M + H]$^+$ = 337.9683.

To a solution of compound 6-bromo-2-(2-fluoro-5-nitrophenyl)-[1,2,4]triazolo[1,5-a]pyrimidine (6 g, 17.7 mmol) in THF (150 mL) was added Raney Nickel (7 g) and ZnI$_2$ (2.26 g, 7.1 mmol), the suspension was degassed under vacuum, and the mixture was stirred under H$_2$ (50 psi) at 25 °C for 2 h. The mixture was filtered, and the solvents were removed to give the crude product. The crude product was washed with MeOH (50 mL × 2) and dried under vacuum to give compound **12** (4.2 g, 77% yield). ^{1}H NMR (400 MHz, DMSO): 9.93 (d, J = 2.3 Hz, 1H), 8.98 (d, J = 2.0 Hz, 1H), 7.39–7.45 (m, 1H), 6.99–7.10 (m, 1H), 6.67–6.76 (m, 1H), 5.76 (s, 1H), 5.25 (brs, 2H). ^{13}C NMR (101 MHz, DMSO) δ 163.08, 156.52, 154.05, 153.74, 151.32, 145.84, 137.87, 118.03, 117.91, 117.80, 117.73, 117.56, 117.33, 114.86, 106.16. HRMS found [M + H]$^+$ = 307.9941, $C_{11}H_8O_2N_5BrF$ predicted [M + H]$^+$ = 307.9942.

N-(4-Fluoro-3-(6-(3-methylpyridin-2-yl)-[1,2,4]triazolo[1,5-a]-pyrimidin-2-yl)phenyl)-2,4-dimethyloxazole-5-carboxamide (1). **Step F**: To a solution of 2,4-dimethyloxazole-5-carboxylic acid (1.92 g, 13.6 mmol) in DMF (50 mL) was added HATU (6.2 g, 16.32 mmol) and DIEA (3.5 g, 27.2 mmol) at room temperature. The mixture was stirred for 30 min, and the compound **12** (4.2 g, 13.6 mmol) was added. The mixture was stirred for 3 h, and water (100 mL) was added. The mixture was filtered, and the filter cake was washed with H_2O (50 mL × 2) and THF (50 mL × 2) and dried to give N-(3-(6-bromo-[1,2,4]triazolo[1,5-a]pyrimidin-2-yl)-4-fluoro-phenyl)-2,4-dimethyloxazole-5-carboxamide (3.1 g, 53%). ^{1}H NMR (400 MHz, DMSO) 10.41 (s, 1 H), 9.97 (s, 1H), 9.02 (brs, 1H), 8.75 (s, 1H), 7.93 (s, 1H), 7.40 (t, J = 9.66 Hz, 1H), 2.50 (s, 3H), 2.39 (s, 3H). ^{13}C NMR (101 MHz, DMSO) δ 162.29, 161.49, 156.86, 156.78, 154.16, 143.51, 139.17, 138.05, 135.52, 124.95, 122.80, 117.67,

117.44, 106.48, 14.29, 13.26. HRMS found [M + H]$^+$ = 431.0259, $C_{17}H_{13}O_2N_6BrF$ predicted [M + H]$^+$ = 431.0262.

Step G: To a solution of compound N-(3-(6-bromo-[1,2,4]-triazolo[1,5-a]pyrimidin-2-yl)-4-fluorophenyl)-2,4-dimethyloxazole-5-carboxamide (3.0 g, 7.0 mmol) in dioxane (60 mL) was added 4,4,4′,4′,5,5,5′,5′-octamethyl-2,2′-bi(1,3,2-dioxaborolane) (7.1 g, 28 mmol), [1,1′-bis(diphenylphosphino)ferrocene]dichloropalladium(II) in complex with dichloromethane (0.5 g, 0.7 mmol), and KOAc (2.0 g, 21 mmol) under N$_2$. This mixture was heated to 100 °C for 16 h. The solvent was removed, and the compound was redissolved in THF and filtered through silica gel. The filtrate was concentrated and triturated with MTBE to give compound (2-(5-(2,4-dimethyloxazole-5-carboxamido)-2-fluorophenyl)-[1,2,4]-triazolo[1,5-a]pyrimidin-6-yl)boronic acid (0.67 g, yield, 24%). ^{1}H NMR: DMSO 400 MHz: 2.40 (s, 3 H), 2.51 (s, 3H), 7.38–7.43 (m, 1 H), 7.92–7.96 (m, 1 H), 8.72–8.79 (m, 2 H), 9.08–9.09 (m, 1 H), 9.45–9.48 (m, 1 H), 10.41 (s, 1 H). ^{13}C NMR (101 MHz, DMSO) δ 162.10, 161.49, 160.65, 158.01, 156.83, 155.93, 155.49, 143.47, 142.17, 139.18, 135.43, 124.85, 122.93, 118.51, 118.39, 117.60, 117.38, 14.28, 13.26. LCMS: [ESI] m/z 397.1 [M − 82 + 1]$^+$. HRMS found [M − 82 + 1]$^+$ = 397.1230, $C_{17}H_{15}O_4N_6BF$ predicted [M − 82 + 1]$^+$ = 397.1226.

N-(4-Fluoro-3-(6-(3-methylpyridin-2-yl)-[1,2,4]triazolo[1,5-a]-pyrimidin-2-yl)phenyl)-2,4-dimethyloxazole-5-carboxamide (1). To a solution of (2-(5-(2,4-dimethyloxazole-5-carboxamido)-2-fluorophenyl)-[1,2,4]triazolo[1,5-a]pyrimidin-6-yl)boronic acid (100 mg, 0.21 mmol) and 2-bromo-3-methylpyridine (54 mg, 0.31 mmol) in 1,4-dioxane (10 mL) was added 1 N aqueous sodium carbonate (1.1 mL, 1.1 mmol) and [1,1′-bis(diphenylphosphino)ferrocene]-dichloropalladium(II) in complex with dichloromethane (8.5 mg, 0.011 mmol) at room temperature. The reaction was purged with N$_2$ for 1 min and stirred at 80 °C for 16 h. The reaction mixture was diluted with ethyl acetate and washed with saturated NaHCO$_3$ and brine. The organic layer was dried over magnesium sulfate, filtered, and reduced to dryness. The crude product was purified by reverse phase HPLC to afford compound **1** (36 mg) as a white solid. ^{1}H NMR (400 MHz, MeOD) 9.57 (d, J = 2.4 Hz, 1H), 9.14 (d, J = 2.3 Hz, 1H), 8.67 (dd, J = 5.1 Hz, 1.6 Hz, 1H), 8.58 (dd, J = 6.4 Hz, 2.7 Hz, 1H), 8.09 (dd, J = 7.8 Hz, 1.6 Hz, 1H), 7.91 (ddd, J = 8.9 Hz, 4.3 Hz, 2.8 Hz, 1H), 7.63 (dd, J = 7.9 Hz, 5.1 Hz, 1H), 7.34 (dd, J = 10.4 Hz, 9.0 Hz, 1H), 2.56 (s, 6H), 2.48 (s, 3H). ^{13}C NMR (101 MHz, DMSO) δ 161.92 (d, J = 5.1 Hz), 161.03, 156.79, 156.34, 156.25 (d, J = 252.9 Hz), 154.25, 150.73, 147.4, 143.03, 139.26, 138.69, 136.36, 135.02 (d, J = 2.9 Hz), 132.38, 124.31 (d, J = 8.4 Hz), 123.73, 123.62, 122.38, 117.94 (d, J = 12.1 Hz), 117.07 (d, J = 22.7 Hz), 19.34, 13.85, 12.82. LCMS: [ESI] m/z = 444.4 [M + H]$^+$). HRMS found [M + H]$^+$, 444.1577, $C_{23}H_{19}O_2N_7F$ predicted [M + H]$^+$ = 444.1579.

ASSOCIATED CONTENT

Ⓢ Supporting Information

The Supporting Information is available free of charge at https://pubs.acs.org/doi/10.1021/acs.jmedchem.0c00499.

    Molecular formula strings (CSV)

    Experimental procedures and analytical data for synthesis of all compounds and detailed characterization of compound **1** and protocols for in vitro assays and in vivo studies strings (PDF)

Accession Codes

The cryo-EM structure of binding mode of of **1** to *L. tarentolae* proteasome (accession codes: EMD-10472, PDB ID 6TCZ) and *Leishmania tarentolae* proteasome 20S subunit complexed with **1** and bortezomib (accession codes: EMD-10463, PDB ID: 6TD5) have been deposited in EMDB and PDB databases. The authors will release the atomic coordinates upon article publication.

■ AUTHOR INFORMATION

Corresponding Authors

Advait Nagle − *Genomics Institute of the Novartis Research Foundation (GNF), San Diego, California 92121, United States;* orcid.org/0000-0002-9347-8542; Email: anagle@gnf.org

Valentina Molteni − *Genomics Institute of the Novartis Research Foundation (GNF), San Diego, California 92121, United States;* orcid.org/0000-0002-5387-6036; Email: vmolteni@gnf.org

Christian Wiesmann − *Novartis Institutes for Biomedical Research, CH-4056 Basel, Switzerland;* Email: christian.wiesmann@novartis.com

Authors

Agnes Biggart − *Genomics Institute of the Novartis Research Foundation (GNF), San Diego, California 92121, United States*

Celine Be − *Novartis Institutes for Biomedical Research, CH-4056 Basel, Switzerland*

Honnappa Srinivas − *Novartis Institutes for Biomedical Research, CH-4056 Basel, Switzerland*

Andreas Hein − *Novartis Institutes for Biomedical Research, CH-4056 Basel, Switzerland*

Diana Caridha − *Experimental Therapeutics, Walter Reed Army Institute of Research, Silver Spring, Maryland 20910, United States*

Richard J. Sciotti − *Experimental Therapeutics, Walter Reed Army Institute of Research, Silver Spring, Maryland 20910, United States*

Brandon Pybus − *Experimental Therapeutics, Walter Reed Army Institute of Research, Silver Spring, Maryland 20910, United States*

Mara Kreishman-Deitrick − *Experimental Therapeutics, Walter Reed Army Institute of Research, Silver Spring, Maryland 20910, United States*

Badry Bursulaya − *Genomics Institute of the Novartis Research Foundation (GNF), San Diego, California 92121, United States*

Yin H. Lai − *Genomics Institute of the Novartis Research Foundation (GNF), San Diego, California 92121, United States*

Mu-Yun Gao − *Genomics Institute of the Novartis Research Foundation (GNF), San Diego, California 92121, United States*

Fang Liang − *Genomics Institute of the Novartis Research Foundation (GNF), San Diego, California 92121, United States*

Casey J. N. Mathison − *Genomics Institute of the Novartis Research Foundation (GNF), San Diego, California 92121, United States;* orcid.org/0000-0002-1310-826X

Xiaodong Liu − *Genomics Institute of the Novartis Research Foundation (GNF), San Diego, California 92121, United States*

Vince Yeh − *Genomics Institute of the Novartis Research Foundation (GNF), San Diego, California 92121, United States*

Jeffrey Smith − *Genomics Institute of the Novartis Research Foundation (GNF), San Diego, California 92121, United States*

Isabelle Lerario − *Genomics Institute of the Novartis Research Foundation (GNF), San Diego, California 92121, United States*

Yongping Xie − *Genomics Institute of the Novartis Research Foundation (GNF), San Diego, California 92121, United States*

Donatella Chianelli − *Genomics Institute of the Novartis Research Foundation (GNF), San Diego, California 92121, United States*

Michael Gibney − *Genomics Institute of the Novartis Research Foundation (GNF), San Diego, California 92121, United States*

Ashley Berman − *Genomics Institute of the Novartis Research Foundation (GNF), San Diego, California 92121, United States*

Yen-Liang Chen − *Novartis Institute of Tropical Diseases, Emeryville, California 94608, United States*

Jan Jiricek − *Novartis Institute of Tropical Diseases, Emeryville, California 94608, United States*

Lauren C. Davis − *Genomics Institute of the Novartis Research Foundation (GNF), San Diego, California 92121, United States*

Xianzhong Liu − *Genomics Institute of the Novartis Research Foundation (GNF), San Diego, California 92121, United States*

Jaime Ballard − *Genomics Institute of the Novartis Research Foundation (GNF), San Diego, California 92121, United States*

Shilpi Khare − *Genomics Institute of the Novartis Research Foundation (GNF), San Diego, California 92121, United States*

Fabian Kurt Eggimann − *Novartis Institutes for Biomedical Research, CH-4056 Basel, Switzerland*

Alexandre Luneau − *Novartis Institutes for Biomedical Research, CH-4056 Basel, Switzerland*

Todd Groessl − *Genomics Institute of the Novartis Research Foundation (GNF), San Diego, California 92121, United States*

Michael Shapiro − *Genomics Institute of the Novartis Research Foundation (GNF), San Diego, California 92121, United States*

Wendy Richmond − *Genomics Institute of the Novartis Research Foundation (GNF), San Diego, California 92121, United States*

Kevin Johnson − *Genomics Institute of the Novartis Research Foundation (GNF), San Diego, California 92121, United States*

Patrick J. Rudewicz − *Novartis Institute of Tropical Diseases, Emeryville, California 94608, United States*

Srinivasa P. S. Rao − *Novartis Institute of Tropical Diseases, Emeryville, California 94608, United States;* orcid.org/0000-0002-7156-5725

Christopher Thompson − *Novartis Institutes for Biomedical Research, Cambridge, Massachusetts 02139, United States*

Tove Tuntland − *Genomics Institute of the Novartis Research Foundation (GNF), San Diego, California 92121, United States*

Glen Spraggon − *Genomics Institute of the Novartis Research Foundation (GNF), San Diego, California 92121, United States*

Richard J. Glynne − *Genomics Institute of the Novartis Research Foundation (GNF), San Diego, California 92121, United States*

Frantisek Supek − *Genomics Institute of the Novartis Research Foundation (GNF), San Diego, California 92121, United States*

■ ABBREVIATIONS

PSMB, proteasome subunit beta type; cryo-EM, cryogenic electron microscopy; VL, visceral leishmaniasis; ER, extraction ratio; HT, high throughput; FASSIF, fasted state simulated intestinal fluid; qPCR, quantitative polymerase chain reaction; EC_{50}, half maximal effective concentration; IC_{50}, half-maximum inhibitory concentration; PO, oral administration; IV, intravenous; b.i.d., twice a day; q.d., once daily ("quaque die"); AUC, area under the curve; DN AUC, dose normalized area under the curve; MRT, mean residence time; PK-PD, pharmacokinetic-pharmacodynamics; SD, standard deviation; SEM, standard error of the mean; MNT, micronucleus test; GPCR, G-protein coupled receptor; VMAT2, vesicular mono-amine transporter 2; CYP, cytochrome P; HRMS, high-resolution mass spectrometry; LCMS, liquid chromatography mass spectrometry; ESI, electrospray ionization

■ REFERENCES

(1) Nagle, A. S.; Khare, S.; Kumar, A. B.; Supek, F.; Buchynskyy, A.; Mathison, C. J.; Chennamaneni, N. K.; Pendem, N.; Buckner, F. S.; Gelb, M. H.; Molteni, V. Recent developments in drug discovery for leishmaniasis and human African trypanosomiasis. *Chem. Rev.* **2014**, *114*, 11305−11347.

(2) Pandey, K.; Pal, B.; Siddiqui, N. A.; Rabi Das, V. N.; Murti, K.; Lal, C. S.; Verma, N.; Babu, R.; Ali, V.; Kumar, R.; Das, P. Efficacy and safety of liposomal Amphotericin B for visceral leishmaniasis in children and adolescents at a tertiary care center in Bihar, India. *Am. J. Trop. Med. Hyg.* **2017**, *97*, 1498−1502.

(3) Sundar, S.; Singh, A. Chemotherapeutics of visceral leishmaniasis: present and future developments. *Parasitology* **2018**, *145*, 481−489.

(4) Wasunna, M.; Njenga, S.; Balasegaram, M.; Alexander, N.; Omollo, R.; Edwards, T.; Dorlo, T. P.; Musa, B.; Ali, M. H.; Elamin, M. Y.; Kirigi, G.; Juma, R.; Kip, A. E.; Schoone, G. J.; Hailu, A.; Olobo, J.; Ellis, S.; Kimutai, R.; Wells, S.; Khalil, E. A.; Strub Wourgaft, N.; Alves, F.; Musa, A. Efficacy and safety of AmBisome in combination with sodium stibogluconate or miltefosine and miltefosine monotherapy for African visceral leishmaniasis: phase II randomized trial. *PLoS Neglected Trop. Dis.* **2016**, *10*, e0004880.

(5) Sundar, S.; Chakravarty, J. Antimony toxicity. *Int. J. Environ. Res. Public Health* **2010**, *7*, 4267−4277.

(6) Khare, S.; Nagle, A. S.; Biggart, A.; Lai, Y. H.; Liang, F.; Davis, L. C.; Barnes, S. W.; Mathison, C. J.; Myburgh, E.; Gao, M. Y.; Gillespie, J. R.; Liu, X.; Tan, J. L.; Stinson, M.; Rivera, I. C.; Ballard, J.; Yeh, V.; Groessl, T.; Federe, G.; Koh, H. X.; Venable, J. D.; Bursulaya, B.; Shapiro, M.; Mishra, P. K.; Spraggon, G.; Brock, A.; Mottram, J. C.; Buckner, F. S.; Rao, S. P.; Wen, B. G.; Walker, J. R.; Tuntland, T.; Molteni, V.; Glynne, R. J.; Supek, F. Proteasome inhibition for treatment of leishmaniasis, Chagas disease and sleeping sickness. *Nature* **2016**, *537*, 229−233.

(7) Wyllie, S.; Brand, S.; Thomas, M.; De Rycker, M.; Chung, C. W.; Pena, I.; Bingham, R. P.; Bueren-Calabuig, J. A.; Cantizani, J.; Cebrian, D.; Craggs, P. D.; Ferguson, L.; Goswami, P.; Hobrath, J.; Howe, J.; Jeacock, L.; Ko, E. J.; Korczynska, J.; MacLean, L.; Manthri, S.; Martinez, M. S.; Mata-Cantero, L.; Moniz, S.; Nuhs, A.; Osuna-Cabello, M.; Pinto, E.; Riley, J.; Robinson, S.; Rowland, P.; Simeons, F. R. C.; Shishikura, Y.; Spinks, D.; Stojanovski, L.; Thomas, J.; Thompson, S.; Viayna Gaza, E.; Wall, R. J.; Zuccotto, F.; Horn, D.; Ferguson, M. A. J.; Fairlamb, A. H.; Fiandor, J. M.; Martin, J.; Gray, D. W.; Miles, T. J.; Gilbert, I. H.; Read, K. D.; Marco, M.; Wyatt, P. G. Preclinical candidate for the treatment of visceral leishmaniasis that acts through proteasome inhibition. *Proc. Natl. Acad. Sci. U. S. A.* **2019**, *116*, 9318−9323.

(8) Berghausen, J.; Faller, B. Diagnosing solubility limitations − the example of hydrate formation. *ADMET DMPK* **2014**, *2*, 115−125.

(9) Ishikawa, M.; Hashimoto, Y. Improvement in aqueous solubility in small molecule drug discovery programs by disruption of molecular planarity and symmetry. *J. Med. Chem.* **2011**, *54*, 1539−1554.

(10) Higashino, H.; Hasegawa, T.; Yamamoto, M.; Matsui, R.; Masaoka, Y.; Kataoka, M.; Sakuma, S.; Yamashita, S. In vitro-in vivo correlation of the effect of supersaturation on the intestinal absorption of BCS class 2 drugs. *Mol. Pharmaceutics* **2014**, *11*, 746−754.

(11) Skolnik, S. M.; Geraci, G. M.; Dodd, S. Automated supersaturation stability assay to differentiate poorly soluble compounds in drug discovery. *J. Pharm. Sci.* **2018**, *107*, 84−93.

(12) Yardley, V.; Croft, S. L. A comparison of the activities of three Amphotericin B lipid formulations against experimental visceral and cutaneous leishmaniasis. *Int. J. Antimicrob. Agents* **2000**, *13*, 243−248.

(13) Schrader, J.; Henneberg, F.; Mata, R. A.; Tittmann, K.; Schneider, T. R.; Stark, H.; Bourenkov, G.; Chari, A. The inhibition mechanism of human 20S proteasomes enables next-generation inhibitor design. *Science* **2016**, *353*, 594−598.

(14) Huber, E. M.; Heinemeyer, W.; Groll, M. Bortezomib-resistant mutant proteasomes: structural and biochemical evaluation with carfilzomib and ONX 0914. *Structure* **2015**, *23*, 407−417.

(15) Ishiyama, T.; Murata, M.; Miyaura, N. Palladium(0)-catalyzed cross-coupling reaction of alkoxydiboron with haloarenes - a direct procedure for arylboronic esters. *J. Org. Chem.* **1995**, *60*, 7508−7510.

(16) Drugs for neglected diseases initiative. https://www.dndi.org/diseases-projects/leishmaniasis/leish-target-product-profile/ (accessed 2020-05-05).

(17) Li, H.; O'Donoghue, A. J.; van der Linden, W. A.; Xie, S. C.; Yoo, E.; Foe, I. T.; Tilley, L.; Craik, C. S.; da Fonseca, P. C.; Bogyo, M. Structure- and function-based design of plasmodium-selective proteasome inhibitors. *Nature* **2016**, *530*, 233−236.

(18) Buac, D.; Shen, M.; Schmitt, S.; Kona, F. R.; Deshmukh, R.; Zhang, Z.; Neslund-Dudas, C.; Mitra, B.; Dou, Q. P. From bortezomib to other inhibitors of the proteasome and beyond. *Curr. Pharm. Des.* **2013**, *19*, 4025−4038.